Drift of elastic floating ice sheets by waves and current

Kostikov, Vasily; Hayatdavoodi, Masoud; Ertekin, R. Cengiz

Published in:
Physics of Fluids

DOI:
10.1063/5.0091538

Publication date:
2022

Document Version
Peer reviewed version

Drift of elastic floating ice sheets by waves and current: multiple sheets[a)]

Vasily K. Kostikov,[1] Masoud Hayatdavoodi,[2, b)] and R. Cengiz Ertekin[3]

[1)] *College of Shipbuilding Engineering, Harbin Engineering University, Harbin, China*

[2)] *School of Science and Engineering, University of Dundee, Dundee DD1 4HN, UK*

and College of Shipbuilding Engineering, Harbin Engineering University, Harbin, China

[3)] *Ocean & Resources Engineering Department, University of Hawaii, Honolulu, HI 96822, USA*

and College of Shipbuilding Engineering, Harbin Engineering University, Harbin, China

(Dated: 4 May 2022)

A nonlinear theoretical model for deformations, oscillations and drift motions of multiple elastic ice sheets in shallow waters due to combined nonlinear waves and uniform current is presented. The model is based on the Green-Naghdi theory for the fluid motion and the thin plate theory for the deformation of the ice sheets. In principle, there are N number of the floating sheets with arbitrary lengths, drafts, and rigidities, which may be located at arbitrary distances from each other. Nonlinear waves of solitary and cnoidal types are considered, and there are no restrictions on the wave properties (wave height or wave period). The sheets, located at different positions, are shown to drift with different speeds, but surge in most of the wave conditions with equal amplitudes. It is shown systematically that wavelength and spacing between the sheets are the critical parameters determining the drift response of a set of freely floating ice sheets. When wavelength is equal to the distance between the centers of the sheets, they bend and drift in resonance, causing the largest wave reflection. The ambient current is found to affect the drift motion of the sheets nonlinearly. This work complements the Part I paper of the same title, where drift motion of a single ice sheet was investigated.

[a)] Under consideration for publication in Physics of Fluids, AIP.

[b)] Corresponding Author; Electronic mail: mhayatdavoodi@dundee.ac.uk

I. INTRODUCTION

Polar ice regions are often formed by collections of floes, surrounding ships and floating offshore structures which operate in close proximity to other floating structures like breakwaters, buoys or supply vessels (Amdahl, 2019). Melting of the polar ice due to climate change has increased the separation between the ice floes (Feltham, 2015) and thus have added to the importance of considering multiple floating ice sheets in the vicinity of each other and other structures. Multiple floating objects can be found not only in the polar marine field but also in offshore engineering and renewable energy production (López et al., 2021): floating solar photovoltaic panels are fixed to the buoyant structures assembled into grid systems, floating wind turbines are commonly arranged into wind farms, floating airports are often surrounded by breakwaters to reduce the impact of waves on these structures. Thus, considering a set of floating objects, rather than a single isolated body, becomes relevant. In this paper, the model constructed for a single sheet presented in (Kostikov et al., 2021b), hereafter referred to as Part I, is extended to N number of sheets located at arbitrary distances from each other.

The interaction of waves with a collection of deformable plates floating on the water surface has become the subject of extensive research in recent decades. The problem has been solved by use of various numerical approaches, e.g., boundary element method (Ogasawara and Sakai, 2006), the linear wave theory coupled with small-amplitude structural response assumption (Kar et al., 2020), eigenfunction expansion method (Kohout et al., 2007; Zheng et al., 2020), Green-Naghdi (GN hereafter) theory (Kostikov et al., 2021a). Vast majority of theoretical studies on interaction of waves with elastic plates use the linear approximations of the governing equations and formulate the boundary-value problem in the frequency domain. Moreover, these studies exploit the common simplifying assumption that floating plates are somehow restricted from moving horizontally. Series of experimental campaigns has been undertaken to investigate the wave transmission and attenuation by arrays of floating discs and validate the existing theoretical models (Bennetts and Williams, 2015; Montiel et al., 2013).

Freely-floating objects can be displaced from their rest positions as a result of the wave action, which can be as large as that of the wind (Wadhams, 1983). In the literature,

the problem of wave-induced drift of floating plates is mostly discussed in the context of ice floe collisions. The earliest theoretical investigation concerned with the drift motion of multiple ice floes was possibly that of Shen and Auckley (Shen and Ackley, 1991), who studied the mechanism of ice growth in the Antarctic and attributed that to the repeated ice floe collisions. They investigated the frequency of floe collisions and its relation to ice concentration, floe size and elastic properties. Shortly after, Rottier (Rottier, 1992) made a rough estimation of the rate at which interaction event between two ice floes occurs and determined it to depend on the ratio between the root-mean-square of the wave height and the amount of open water space between the pair of floes. Yiew et al. (Yiew et al., 2017) conducted the laboratory experiments with two identical disks in waves. They investigated different collision regimes and reported that collisions were forced either by drift or relative surge motion depending on the incident wavelengths. These works have another simplifying concept in common: the drift motion of the ice in waves was approximated by the slope-sliding model. In that approach, it is assumed that wavelengths are much greater than the floe diameter, so that the floes do not modify the wave field and behave as rigid bodies. A subsequent analysis of this model by Grotmaack and Meylan (2006) has shown that in the absence of wave scattering, the drift is invariant for all floating objects. In practice, however, the drift speed changes based on the size and form of the floating bodies, shown for example through the laboratory experiments of Harms (1987), McGovern and Bai (2014) and Wang et al. (2020a).

Herman (Herman, 2011, 2018) investigated the collision patterns in the ice-covered ocean making an assumption that sea ice possesses the properties of a granular material. In Herman's model, the motion of arbitrary number of ice floes was prescribed by momentum equations with floe size dependent force terms. This approach is rather to assist in understanding the processes of cluster formations in sea ice than to reproduce in details the drift motion of individual ice floes and their effect on the wave field.

It follows from the above that the models on the drift response of floating elastic sheets to nonlinear incident waves presented till recently in the literature are limited in a number of regards, and more insights into the topic are required. Recently, Wu et al. (2021) studied numerically and experimentally the response of a single rigid ice floe to the wave action. They related the motion of the ice floe in all six degrees of freedom with wavelength, ice

thickness and ice shape. Tavakoli and Babanin (2021) investigated the role of dissipation when the rigid plate drifts in viscous fluid with the tool of computational fluid dynamics. They pointed out that the problem becomes more important for elastic multi-body system, such as an array of ice floes. All of these demonstrate the relevance of the subject considered here.

In this work, we propose the method based on the Level I GN equations for simulation of the drift motion and oscillations of multiple elastic ice sheets under the action of nonlinear waves and uniform current prior to collision. In this method, the horizontal trajectories of the sheets are found from Newton's second law of motion with horizontal forces obtained through integrating the hydrodynamic pressure along the wetted surface of the sheets. This is a complementary Part II to our previous study in Part I, where the case of a single sheet was investigated. The rest of the paper is organized as follows. In section II, the problem statement is reformulated for the case of multiple sheets and an overview of the governing equations is given. In subsequent sections III-VI, results and discussion are provided for the following four different perspectives: (III) time series of basic kinematic and dynamic indicators, including horizontal trajectories, horizontal velocities and horizontal hydrodynamic forces; (IV) velocity and pressure fields; (V) time-averaged surge oscillation heights and net drift speeds; (VI) reflection and transmission coefficients. The sections are organized into subsections, where cnoidal wave without current, cnoidal wave with current, and, where appropriate, solitary wave are considered. Finally, in the last section, conclusions are summarized based on the various effects observed in the model.

II. THE GOVERNING EQUATIONS

Fluid motion is assumed to be governed by the Level I Green-Naghdi equations (Green and Naghdi, 1976a). In this approach, originally developed based on the theory of directed fluid sheets (see Green et al. (1974), Green and Naghdi (1976b)), the fluid is assumed inviscid and incompressible, but irrotationality of the flow is not required (although a special version of the equations are later obtained by Kim and Ertekin (2000) and Kim et al. (2001) for irrotational flows). The GN equations, satisfy the nonlinear free surface boundary conditions, and postulate the conservation laws exactly (some averaged along the water

column). In this theory, the form of the velocity field across the water column is prescribed, and this form determines the level of the equations. In the Level I GN equations, used in this study, the vertical velocity varies linearly across the water column, making this form of the equations most applicable to propagation of long waves in shallow waters. High-level GN equations are obtained by considering nonlinear functions for variation of vertical velocity over the water depth, see for example Zhao et al. (2014), Zhao et al. (2015) and Zhao et al. (2019). More discussion about various forms of the GN equations can be found in (Ertekin et al., 2014). See Hayatdavoodi et al. (2015) and Hayatdavoodi et al. (2019) for practical applications of the GN equations on wave loads on structures, (Wang et al., 2020b) and (Zhao et al., 2020) for nonlinear wave-current interaction by the GN equations, subjects of interest to this study.

In this study, a set of N elastic sheets floating freely on the surface of an inviscid fluid is considered in a two-dimensional Cartesian reference frame in which the x axis is pointing to the right, the y axis is directed upwards, and its origin is located on the undisturbed free surface. The sheets have lengths L_i, thicknesses δ_i, masses per unit width m_i, drafts d_i, and flexural rigidities D_i, and are initially at rest, where subscript $1 \leq i \leq N$ is used for sheet identification. The fluid is inviscid and incompressible, has constant density ρ and depth h (figure 1). The depth of the fluid under the i-th sheet at rest is $h_i = h - d_i$.

A numerical wave tank is created, where nonlinear waves of solitary and cnoidal types with given properties, and uniform current are generated. Sheets are free to move horizontally (with respect to the stationary seafloor) with arbitrary velocities as a result of the combined wave-current action. Hence, the initial distance parameter l_i between i-th and $(i+1)$-th sheets should be distinguished from the distance $l_i(t)$ at any given time. In the next sections, the sheets will be referenced as *sheet* i in a sequential order from left to right or, in the special case of two sheets, as *upstream sheet* and *downstream sheet*.

Similar to Part I, it is assumed that the elastic sheets are directly in touch with the fluid at all times (no air gaps are allowed), the friction at the contact surfaces is assumed negligible (the force on the sheets is limited to hydrodynamic pressure only), the fluid is not allowed to flow on the upper surface of the sheet (no overtopping), all points of the sheets move with equal horizontal speeds (any possible deformation occurring in the sheet is limited to the vertical bending), and non-colliding motion of the sheets is considered. The equations,

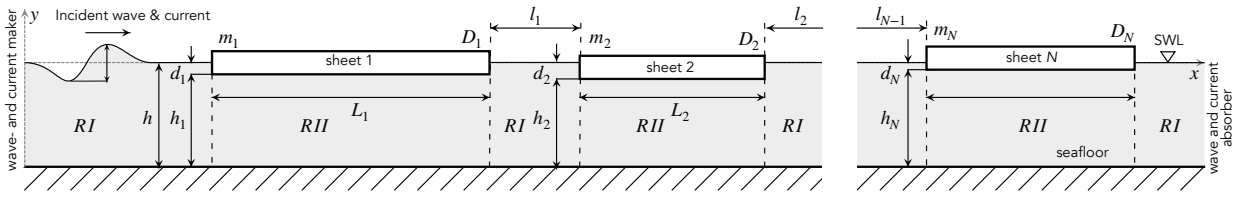

FIG. 1. Schematic view of the problem of waves and current interaction with a set of N deformable floating sheets with arbitrary properties, and the two types of fluid regions referred to in the text.

as well as computed results, are presented in dimensionless forms after using ρ, h and g as a dimensionally independent set, where g is the acceleration due to gravity. Henceforth, all variables, unknown functions and parameters are dimensionless unless otherwise stated.

The mathematical model for a single elastic sheet has been presented in Part I. In this work we extend this model to the case of multiple sheets. Following the same principle, the flow domain is decomposed into the regions of two types, namely RI under free surface, and RII under each of the sheets. The flow in each region is governed by its own set of equations. The solution is obtained by alternately connecting Regions RI and RII and solving the equations simultaneously in the entire fluid domain. In order to complete the formulation of the problem, we summarize the equations of motion, matching and boundary conditions, specified in each region. This method of decomposing the domain into regions has been successfully used by Hayatdavoodi & Ertekin (Hayatdavoodi and Ertekin, 2015a,c) to study solitary and cnoidal waves interaction with a submerged plate.

The basic equations governing the fluid motion throughout the whole domain are provided by the Level I GN theory (Green and Naghdi, 1976a,b). In Region RI formed by a flat and stationary seafloor and the free surface (on top of which the pressure is atmospheric and assumed zero here), the equations of motion are written in dimensionless form as (Ertekin, 1984; Ertekin et al., 1986):

$$\eta_{,t} + (1+\eta)u_{,x} + u\eta_{,x} = 0, \tag{1}$$

$$3\dot{u} + 3\eta_{,x} + 2\eta_{,x}\ddot{\eta} + (1+\eta)\ddot{\eta}_{,x} = 0, \tag{2}$$

$$v(x,y,t) = \dot{\eta}(1+y)/(1+\eta), \tag{3}$$

$$p(x,y,t) = \frac{1}{2}(1+\eta)(\ddot{\eta}+2) - (1+y) - \frac{1}{2}(1+y)^2\ddot{\eta}/(1+\eta). \tag{4}$$

Subscripts after comma denote partial derivatives with respect to the given variable and

upper dot specifies the total time (or material) derivative. Unknown free surface elevation $\eta(x,t)$, measured from the still water level (SWL), and horizontal fluid velocity $u(x,t)$ can be found from equations (1)-(2), representing conservation of mass and conservation of linear momentum, respectively. Vertical fluid velocity $v(x,y,t)$ and hydrodynamic pressure $p(x,y,t)$ can then be expressed explicitly from relations (3)-(4). Similarly, in Region RII formed by a flat and stationary seafloor and the floating elastic surface on the top the equations of motion are formulated as (Xia et al., 2008; Ertekin and Xia, 2014; Kostikov et al., 2021a):

$$\zeta_{,t} + (h_i + \zeta)u_{,x} + u\zeta_{,x} = 0, \tag{5}$$

$$3\dot{u} + 3\zeta_{,x} + 3\hat{p}_{,x} + 2\zeta_{,x}\ddot{\zeta} + (h_i + \zeta)\ddot{\zeta}_{,x} = 0, \tag{6}$$

$$\hat{p} - m_i(1 + \zeta_{,tt}) - D_i\zeta_{,xxxx} = 0, \tag{7}$$

$$v(x,y,t) = \dot{\zeta}(1+y)/(h_i + \zeta), \tag{8}$$

$$p(x,y,t) = \frac{1}{2}(h_i + \zeta)(\ddot{\zeta} + 2) + \hat{p} - (1+y) - \frac{1}{2}(1+y)^2\ddot{\zeta}/(h_i + \zeta). \tag{9}$$

Unknown plate deformation $\zeta(x,t)$, measured from its stationary position, horizontal fluid velocity $u(x,t)$, and fluid pressure at the fluid-sheet contact surface $\hat{p}(x,t)$ can be found from equations (5)-(7), representing conservation of mass, conservation of linear momentum and the equation of thin plate theory (Timoshenko and Woinowsky-Krieger, 1959), respectively. The flexural rigidity of the sheet is defined through its thickness δ_i, Young's modulus E_i and Poisson's ratio ν_i by $D_i = E_i\delta_i^3/12(1-\nu_i^2)$. Vertical fluid velocity $v(x,y,t)$ and total pressure $p(x,y,t)$ in RII can be then expressed explicitly from relations (8)-(9).

The sheets, which are allowed to float freely, can be displaced from their initial positions, causing the displacement of Regions RI and RII. Therefore the basic equations (1)-(9) should be complemented by momentum equation prescribing the translational motion of the sheets:

$$m_i L_i \frac{d^2 X_i}{dt^2} = -\int_{x_i^L}^{x_i^T} \hat{p}(x,t)\zeta_{,x}dx + (\hat{p}(x_i^L,t) - \hat{p}(x_i^T,t))\frac{d}{2} + F_d(t). \tag{10}$$

Here X_i denotes the horizontal coordinate of the i-th sheet. The only driving force for the drifting sheets in an inviscid fluid is the hydrodynamic load resulting from the gradient of pressure around the sheet. The integral term in equation (10) is the force due to hydrodynamic pressure acting along the lower surface of the sheet. The second term is the force due

to the hydrodynamic pressure distribution along the vertical walls of the sheets down to the edges, which is assumed to be mostly linear in Level I GN theory, see Hayatdavoodi et al. (2018); Neill et al. (2018) for discussion on this. The last term is the drag force caused by friction between the body and the fluid, expressed by (Shen and Ackley, 1991):

$$F_d(t) = c_d S_i (u - U_i(t))|u - U_i(t)|, \tag{11}$$

where c_d is the drag coefficient, S_i is the wetted surface area of the sheet and U_i is the horizontal speed of the sheet. Since we stay in the framework of the inviscid fluid, the drag force is assumed negligible. This assumption is substantiated by the results of the slope-sliding model, showing that surge motion of the plate is insensitive to the value of the drag coefficient (Meylan et al., 2015) and the drift speed depends only marginally on it (Grotmaack and Meylan, 2006). For the detailed discussion of equation (10) without the drag term the reader is referred to Part I.

Due to the presence of elastic surfaces with non-zero draft, the fluid particle velocity $u(x,t)$ and its derivatives become discontinuous at the interfaces between regions. The solutions obtained in each region should be connected through appropriate jump and matching conditions to ensure continuity of mass, momentum and energy across the discontinuity curves. At the leading ($x = x_i^L$) and trailing ($x = x_i^T$) edges of the sheets the following conditions should be satisfied:

$$\zeta_{,xx} = 0, \quad 3\zeta_{,x}u_{,xx} + (h_i + \zeta)u_{,xxx} = 0, \tag{12}$$

$$\zeta_{,xxx} = 0, \quad 4\zeta_{,x}u_{,xxx} + (h_i + \zeta)u_{,xxxx} + \zeta_{,xxx}(u - U_i) = 0, \tag{13}$$

$$\eta(u - U_i)|_{x_i^L - 0} = \zeta(u - U_i)|_{x_i^L + 0}, \quad \frac{1+\eta}{2}(\ddot{\eta} + 2)|_{x_i^L - 0} = \Big[\frac{h_i + \zeta}{2}(\ddot{\zeta} + 2) + \hat{p}\Big]_{x_i^L + 0}, \tag{14}$$

$$\zeta(u - U_i)|_{x_i^T - 0} = \eta(u - U_i)|_{x_i^T + 0}, \quad \Big[\frac{h_i + \zeta}{2}(\ddot{\zeta} + 2) + \hat{p}\Big]_{x_i^T - 0} = \frac{1+\eta}{2}(\ddot{\eta} + 2)|_{x_i^T + 0}. \tag{15}$$

Here, $x_i^L \pm 0$ and $x_i^T \pm 0$ denote the single-sided limiting values of x_i^L and x_i^T, respectively. Equations (12)-(13) formulated above represent the vanishing bending moments and shear stresses, respectively, together with their effect on mass continuity equation (5). This is because each sheet is a free-free beam. Equations (14)-(15) represent continuity of mass flux and bottom pressure across the discontinuity curves between the regions at the leading and trailing edges, correspondingly. It is worth mentioning, that there is no need to include

explicitly the exact nonlinear kinematic and dynamic boundary conditions at the upper surfaces of Regions RI and RII. Due to the intrinsic properties of GN equations, these boundary conditions as well as the impermeability condition on the bottom are already enforced in the system of equations (1)–(9). A complete discussion of the GN jump conditions around a plate can be found in Appendix of (Hayatdavoodi and Ertekin, 2015b).

On the left side of the domain, a numerical wave- and current-maker generates periodic nonlinear waves (cnoidal waves) of height H and length λ with an optional uniform current of constant speed U_c. The periodic solution of equations (1)-(2) can be written in the moving coordinate system as (Sun, 1991; Ertekin and Becker, 1998; Hayatdavoodi and Ertekin, 2015c):

$$\eta(x-ct) = \eta_2 + H\mathbf{Cn}^2, \quad u(x-ct) = \frac{c\cdot\eta(x-ct)}{1+\eta(x-ct)}, \tag{16}$$

where $\mathbf{Cn}$ is the Jacobian elliptic function and c is the phase speed, obtained by solving the following relations iteratively:

$$c = \sqrt{(1+\eta_1)(1+\eta_2)(1+\eta_3)} \tag{17}$$

$$\eta_1 = -\frac{H}{k^2}\frac{E}{k}, \quad \eta_2 = \frac{H}{k^2}\left(1-k^2-\frac{E}{k}\right), \quad \eta_3 = \eta_2 + H, \quad k^2 = \frac{H}{\eta_3-\eta_1}. \tag{18}$$

Here K and E are the complete elliptic integrals of the first and second kind, respectively. The wavelength λ can be calculated using the GN dispersive relation:

$$\lambda = ckK\sqrt{\frac{16}{3H}}. \tag{19}$$

When current is present, the wave- and current-maker (absorber) should maintain the corresponding inflow (outflow) in (out of) the flow domain. Hence, the fluid velocity at the wavemaker is prescribed as:

$$u_c(t) = u(x-ct) + U_c. \tag{20}$$

The current is favourable or adverse, when at initial time the fluid moves with uniform speed in the positive ($U_c > 0$) or negative direction ($U_c < 0$), respectively. The initial conditions are formulated as follows:

$$\eta(x,0) = 0, \qquad u(x,0) = U_c \tag{21}$$

In the absence of current ($U_c = 0$) the fluid is initially at rest.

On the right side of the domain, the open-boundary Orlanski's condition is prescribed to reduce reflections back into the wave tank:

$$\eta_{,t} \pm c\eta_{,x} = 0, \quad u_{,t} \pm cu_{,x} = 0. \tag{22}$$

We note that the GN equations, as used here, describe the unsteady motion of inviscid and incompressible fluids. No assumption is made on the nature of fluid motion, whether oscillatory or uniform. Hence, for the wave-current conditions, no changes are required to the governing equations. See e.g. (Wang et al., 2020a) for further discussion on the application and performance of the GN equations to the wave-current interaction problem.

The wave- and current-maker is capable of generating solitary waves of amplitude A as well. An analytical solitary wave solution of the Level I GN equations can be found in (Ertekin, 1984). This solution has been applied to the problems of wave diffraction by submerged plate (Hayatdavoodi and Ertekin, 2015b) and uneven bottom (Ertekin et al., 2014). It will be demonstrated below that the results for a solitary wave are more informative in the case of multiple sheets than in the case of a single sheet.

Two sets of equations (1)-(4) and (5)-(10) supplemented by boundary conditions (12)-(15) formulate fully the coupled motion of the fluid and freely floating elastic sheets. The solution is found with the use of a finite-difference technique. The numerical algorithm follows the principle formulated for the single sheet and extends it to the multiple sheet case by running the code in the combination of regions simultaneously. More details about the theory and approach used in this study, and the numerical solution, can be found in Part I.

III. HORIZONTAL TRAJECTORIES

The primary focus of the present study is on drift motion of multiple sheets with arbitrary properties and located at any distance from each other. Hence, we will investigate the interplay between two parameters of the problem: the number of sheets N and the initial spacing l_i. For this purpose, various sets of equally-sized and equally-spaced sheets in different wave conditions will be examined in subsequent sections. The arrays of arbitrary-sized sheets of arbitrary masses and rigidities non-uniformly distributed on the water surface though approachable by the present model, will be left out of bounds of the current study

for clarity. For the individual effects of sheet properties on its drift motion, as well as the comparisons with experiments and alternative numerical methods in the case of a single sheet, the reader is referred to Part I. In subsequent sections, we will denote the sheets that are free to move horizontally as *free sheets*, and the sheets that are restrained from drift as *fixed sheets*.

Multiple sheets under the action of waves and current may experience different wave forcing, depending on wave conditions, sheet properties and their relative locations. Consequently, free sheets, being initially at rest, start to drift with different speeds, and even in different directions, i.e. exhibit differential drift. The distance dividing the drifting sheets might either increase or decrease, causing changes in their mutual interaction. Hence, compared to a single sheet case, the wave interaction with multiple sheets, is a more complex dynamic process, involving wave-sheet and sheet-sheet interactions. In this section, we will consider the trajectories of the sheets and study the mechanisms governing the differential drift.

A. Cnoidal wave without current

To the best of our knowledge, no experimental data or numerical simulations have been reported on non-colliding wave-induced drift motion of multiple elastic sheets in shallow water, which could have been used for comparisons here. The existing works study the elastic bending of the sheets which are fixed in space (Kohout et al., 2007), or investigate the repeated collisions of the sheets set at a close distance to each other (Shen and Ackley, 1991; Yiew et al., 2017). In figure 2, the horizontal trajectory of the upstream sheet in the set of two sheets is compared to the horizontal trajectory of a single sheet, determined through three different approaches: predicted by the present model (Kostikov et al., 2021b), calculated with the SPH method and measured in the laboratory experiments (Ren et al., 2015). The initial distance between the sheets is chosen large enough to avoid collisions, and for larger wave heights should be larger. Figure 2 demonstrates that the presence of the downwave sheet makes the upstream sheet drift slower, compared to the single sheet case, but does not affect the surge oscillations. The modulation in the drift speed of the upstream sheet can be attributed to the wave reflected from the downwave sheet. In our

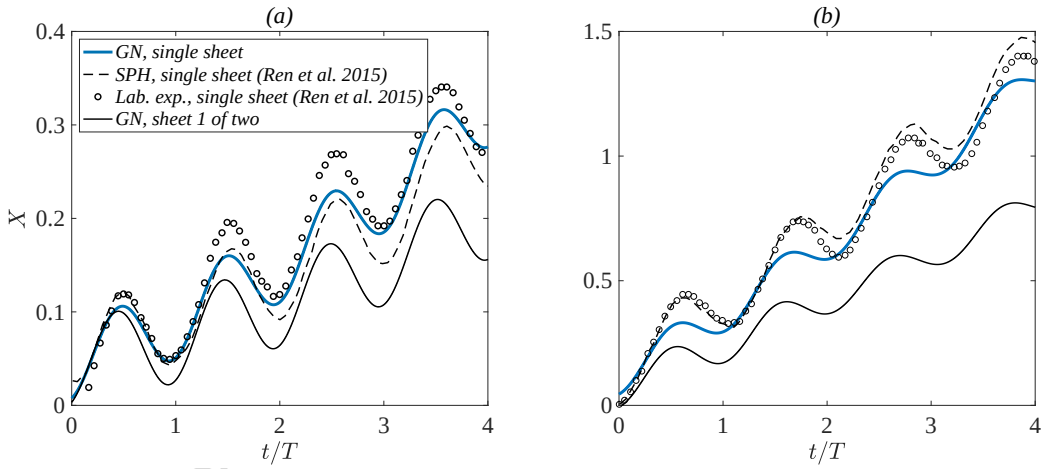

FIG. 2. Comparisons of time series of horizontal trajectories of a freely floating sheet ($L_1 = 0.75$, $m_1 = 0.25$, $D_1 = 1$) and the upstream sheet of the set of two sheets ($L_i = 0.75$, $m_i = 0.25$, $D_i = 1$, $i = 1, 2$) under the action of a regular wave without current of the period $T = 6$ and height: (a) $H = 0.1$ and (b) $H = 0.25$. The initial distance between the sheets: (a) $l_1 = L_1$ and (b) $l_1 = 5L_1$.

approach, we do not include overwash, fluid viscosity and three-dimensional motions of the rigid plate (pitch, sway and yaw), and hence the predicted surge amplitude differs slightly from the laboratory measurements, especially for larger waves. Also, the experiments are conducted on a box-shape object, remarkably different from deformable sheets considered here, and this further adds to the differences.

Figure 3 shows time series of the horizontal trajectories, horizontal velocities and wave-induced horizontal forces of two freely floating sheets initially divided by different distances and acted upon by a cnoidal wave. Because of the fluid gap separating the sheets, there is a phase lag in the oscillations of the horizontal force acting on the downwave sheet. It is observed in figure 3 that, when the wave loads on two sheets are out of phase, the trajectory of the upstream sheet starts to descend due to increased negative drift speed. Compared to the downwave sheet, the horizontal speed and force of the upstream sheet have lower minimums but almost equal maximums. That is, the mismatched forces and speeds oscillate with different amplitudes. When the distance between the centers of the sheets equals to the incoming wavelength, wave loads are matched and both sheets start to move in resonance. In this case, the upstream sheet drifts faster and catches up with the

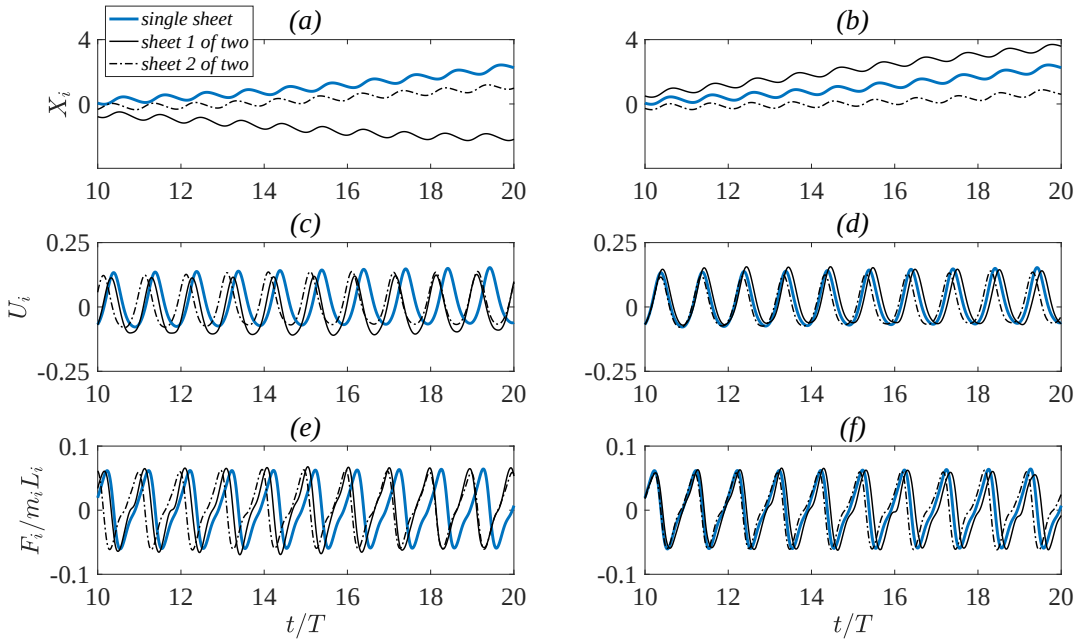

FIG. 3. Time series of (a,b) horizontal trajectories, (c,d) horizontal velocities and (e,f) horizontal forces for two free sheets ($L_i = 3$, $m_i = 0.05$, $D_i = 0.1$, $i = 1, 2$) divided by an initial distance $l_1 = 2L_1$ (left column) and $l_1 = 3L_1$ (right column) under the action of a cnoidal wave ($H = 0.2$, $\lambda/L_1 = 4$) without current. The initial positions of trajectories are placed to zero for comparison purposes.

downwave sheet. As the distance between the sheets is changing gradually, the sheets are switching smoothly from the matched to mismatched regime. Thus, we can conclude that distance between the sheets play pivotal role in their drift movements.

As compared to the case of two sheets discussed above, the multiple sheet clusters, where each element affects the fluid flow both upwave and downwave, have more complex interaction process. Hence, with an increase in the sheet number, it becomes harder to predict their drift motion at any given moment of time. Figure 4 shows time series of horizontal trajectories of six free sheets under the action of cnoidal waves of the same height, but different wavelengths. The sheets, which are uniformly distributed on the fluid surface at the initial time, are scattered as a result of a differential wave action. It is observed in figure 4(a) that the distances between different sheets increase or decrease, so that the total space occupied by the group of sheets change insignificantly. In figure 4(b), the horizontal trajectories of the

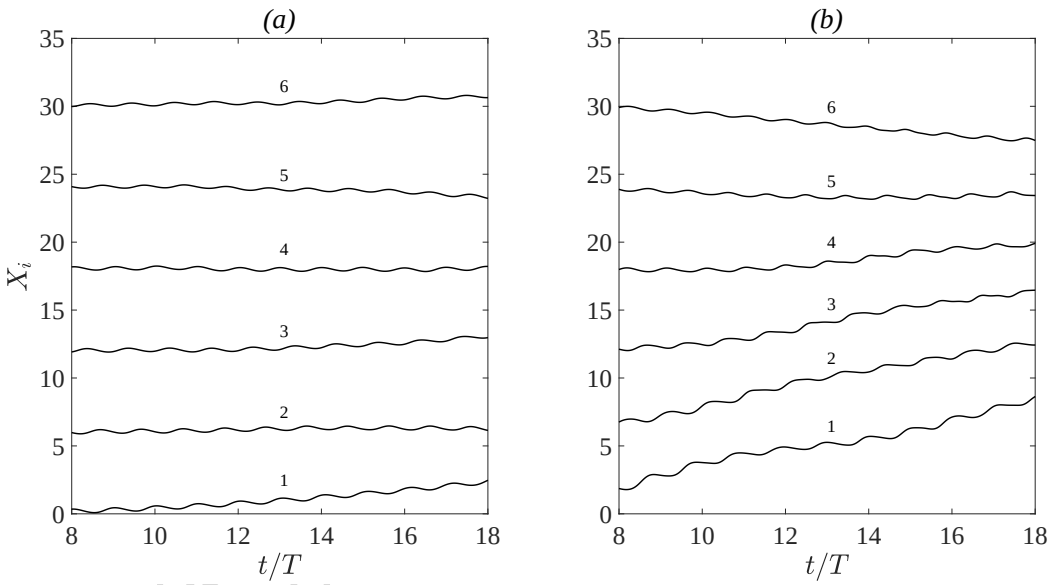

FIG. 4. Time series of horizontal trajectories for six free sheets ($L_i = 3$, $m_i = 0.1$, $D_i = 1$, $i = 1, \ldots, 6$) divided by equal initial distances $l_i = L_1$, ($i = 1, \ldots, 5$) under the action of cnoidal waves without current: (a) $H = 0.2$, $\lambda/L_i = 3$; (b) $H = 0.2$, $\lambda/L_i = 4$. The horizontal trajectories start from the initial positions of the leading edges of the sheets to demonstrate the change in the relative positions of the sheets in subsequent times.

sheets converge together, meaning that the sheets herd together into a band. This complies with Shen & Ackley (Shen and Ackley, 1991), who also observed the herding phenomenon in the slope-sliding model for the group of disk-shaped rigid floes.

Next, we will investigate the transformation in distribution of the sheets on the water surface with time depending on wave conditions and initial spacing parameter. Figure 5 shows lengths of the fluid gaps in the initially uniform cluster of ten sheets at three successive moments of time. A combination of three initial spacings and three wavelengths are considered. The summarized length of the vertical segments of the plots equals to the total open water area contained within the cluster. According to figure 5, when the wavelength is smaller than the initial spacing of the sheet cluster, the sheets are attracted to each other by the action of wave and the distances between them become smaller. When wavelength is equal to the initial spacing of the sheet cluster, the upstream sheets fall behind the rest of the group and the sheets further downstream form the narrow band. For larger wavelength

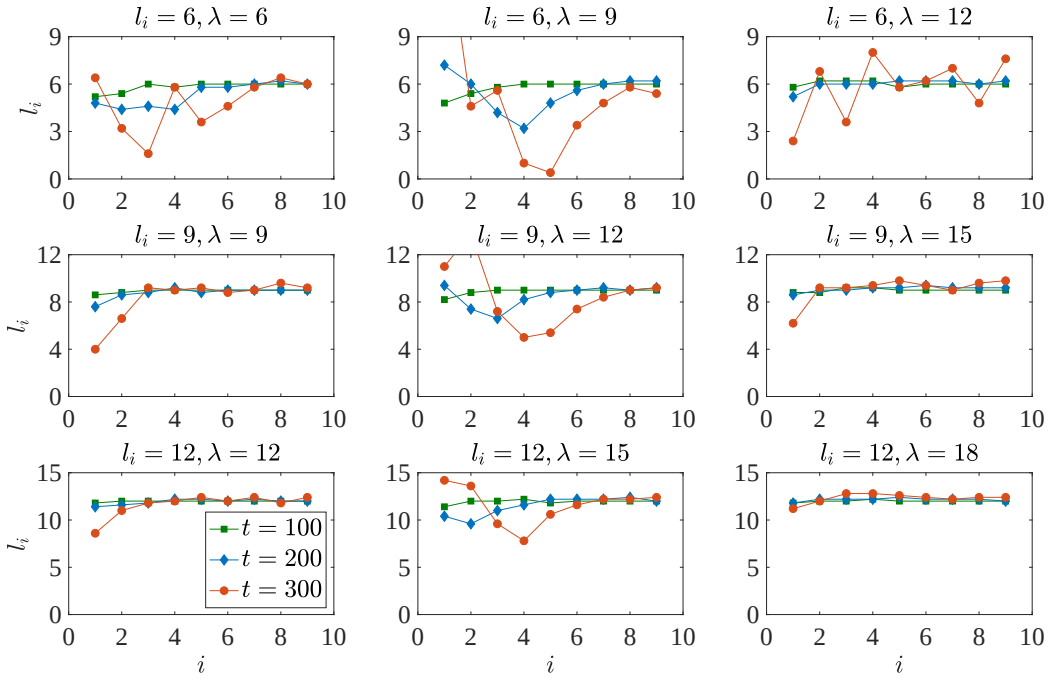

FIG. 5. Distribution of fluid gaps in the cluster of ten sheets ($L_i = 3$, $m_i = 0.1$, $D_i = 1$, $i = 1, \ldots, 10$) with various spacing parameter l_i under the action of a cnoidal wave of various wavelength λ without current at three time moments.

and larger spacing parameter, positions of the sheets relative to each other change little with time, which means that the sheet cluster drifts more as a single unit rather than as separate bodies. With increase in the spacing l_i these effects become weaker.

B. Cnoidal wave with current

To construct a realistic model of ice floe drift, we should consider the joint presence of the wave and current fields. For tracking the individual effects of the current on the drift response of the floating sheets, favourable ($U_c > 0$) or adverse ($U_c < 0$) currents will be considered separately from the pure wave case. Das et al. (Das et al., 2018b,a) studied the wave propagation in a thin elastic plate in deep water approximation and established the phenomenon of wave blocking caused by shear stresses similar to that caused by the opposing current. Barman (Barman et al., 2021) investigated the flexural-gravity wave scattering due

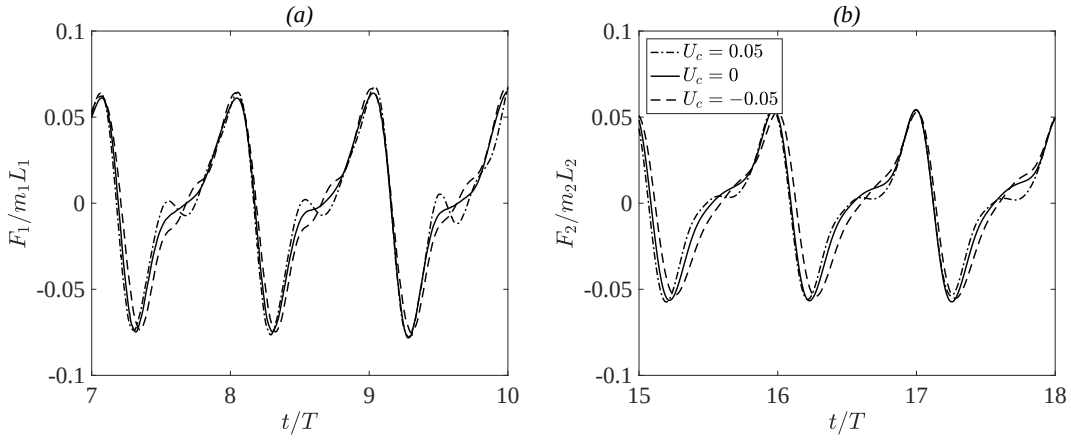

FIG. 6. Time series of horizontal forces on two free sheets ($L_i = 3$, $m_i = 0.1$, $D_i = 1$, $i = 1, 2$), divided by an initial distance $l_1 = 3L_1$, under the action of a cnoidal wave ($H = 0.2$, $\lambda/L_1 = 5$) with and without current: (a) upwave sheet; (b) downwave sheet.

to a crack in an infinite elastic sheet in the presence of compression and studied the case of wave blocking. In the absence of compressive forces in elastic sheets, see equation (7), the occurrence of wave blocking in this study is only possible due to the opposing current. In subsequent analysis, the current speed will be chosen small relative to the speed of the incident wave ($U_c \ll c$), so that the wave propagation on a current without blocking is secured.

Figure 6 shows the contribution of the current to the horizontal forces on two freely floating sheets. The current has little effect on the maximum positive and negative forces, but the correlation between the duration of positive and negative forces changes with the presence of current. Favourable and adverse currents increase the duration of positive and negative forces, respectively.

In figure 7, the drift motions of the two freely floating sheets as a result of the combined wave-current actions are presented. According to the change in the trajectories, the effect of current on the drift response of the set of two sheets is similar to that of the single sheet, discussed in Part I paper (Kostikov et al., 2021b). That is, the favourable current ($U_c > 0$) results in the pair of sheets moving faster when compared to the identical pair of sheets floating in waves without current. On the contrary, the adverse current ($U_c < 0$) slows down the drift movements of the sheets. In two wave cases presented in figure 7, it can be observed

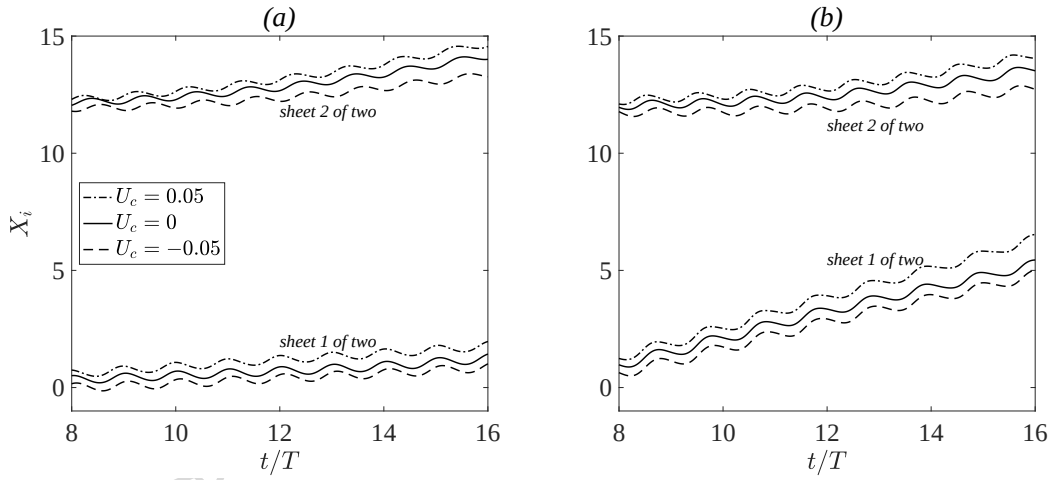

FIG. 7. Time series of horizontal trajectories of two free sheets ($L_i = 3$, $m_i = 0.1$, $D_i = 1$, $i = 1, 2$), divided by an initial distance $l_1 = 3L_1$, under the action of cnoidal waves with and without current: (a) $H = 0.2$, $\lambda/L_1 = 3$; (b) $H = 0.2$, $\lambda/L_1 = 5$. The horizontal trajectories start from the initial positions of the leading edges of the sheets to demonstrate the change in the relative positions of the sheets in subsequent times.

that the effect of favourable current on sheet 1 is stronger than on sheet 2. And inversely, the effect of adverse current on sheet 2 is stronger than on sheet 1.

C. Solitary wave

The conclusions formulated for a cnoidal wave interaction with a single sheet in Part I can be immediately applied to a solitary wave, as it is the limiting case of a very long cnoidal wave of the same height. In case of multiple sheets, the principal advantage of a solitary wave over a cnoidal wave, is that horizontal velocities of the sheets and wave-induced horizontal forces have clear peaks, which allows comparing the effects of the wave on different sheets in the multiple cluster.

Figure 8 represents the solitary wave interaction with a set of three equally distanced sheets in the form of time series of horizontal trajectories, horizontal velocities and wave-induced horizontal forces. Trajectory and velocity plots show that the sheets are set into motion one by one at regular intervals. The sheets stop drifting when the wave peak leaves their surfaces. Compared to a single sheet, the upstream sheet experiences delayed residual

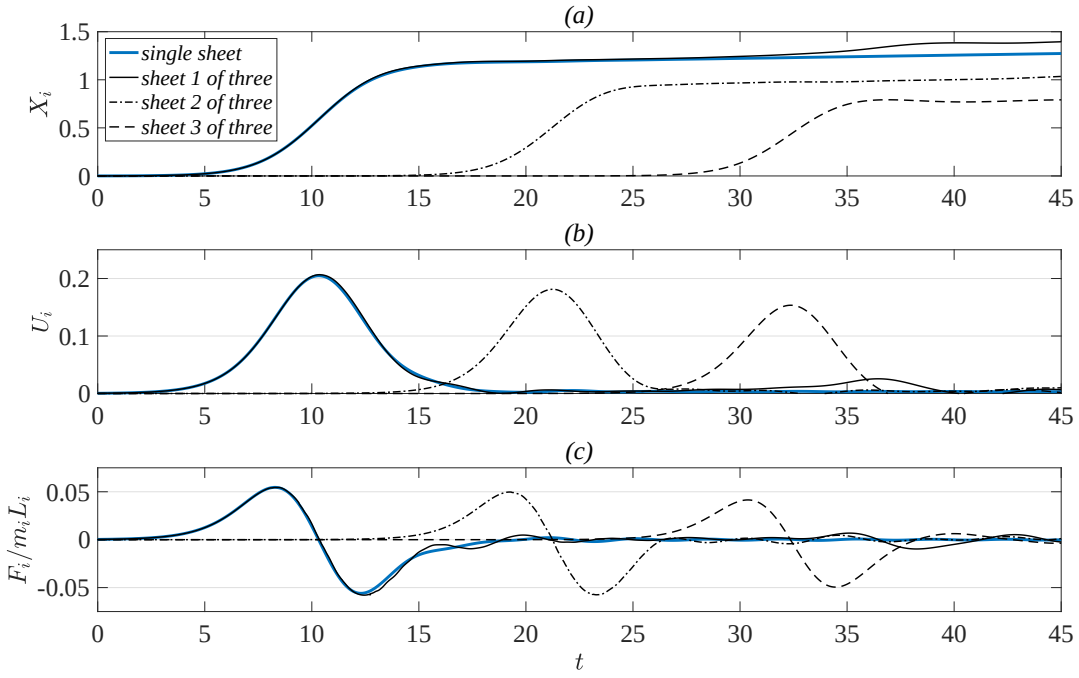

FIG. 8. Time series of (a) horizontal trajectories, (b) horizontal velocities and (c) horizontal forces for three free sheets ($L_i = 3$, $m_i = 0.1$, $D_i = 1$, $i = 1, 2, 3$) initially set at the distances $l_i = 3L_1$ ($i = 1, 2$) under the action of a solitary wave of amplitude $A = 0.2$ without current. The initial positions of trajectories X_i are placed to zero for comparison purposes.

drift due to interaction with the downwave sheets. The force plot demonstrates the attenuation of the wave as it propagates from one sheet to the other: the maximum values of wave-induced horizontal forces and horizontal velocities reduce with increase in the sheet sequence number. As a result, each successive sheet travels to a shorter distance, giving rise to differential drift. By induction, we can conclude that ice concentration in the ice sheet cluster should decrease in the direction of wave propagation.

Figure 9 shows the variations of the peak values of horizontal velocities and maximum wave-induced horizontal forces with the distance parameter l_i for three free sheets considered above. It can be seen that, in terms of maximum wave loads and drift speed, the upstream sheet is not influenced by the presence of the downstream sheets regardless of the distance. This is due to unidirectional action of a solitary wave and very small wave reflection. When the spacings between the sheets is comparable to their lengths ($l_i/L_i < 2$), the wave-induced

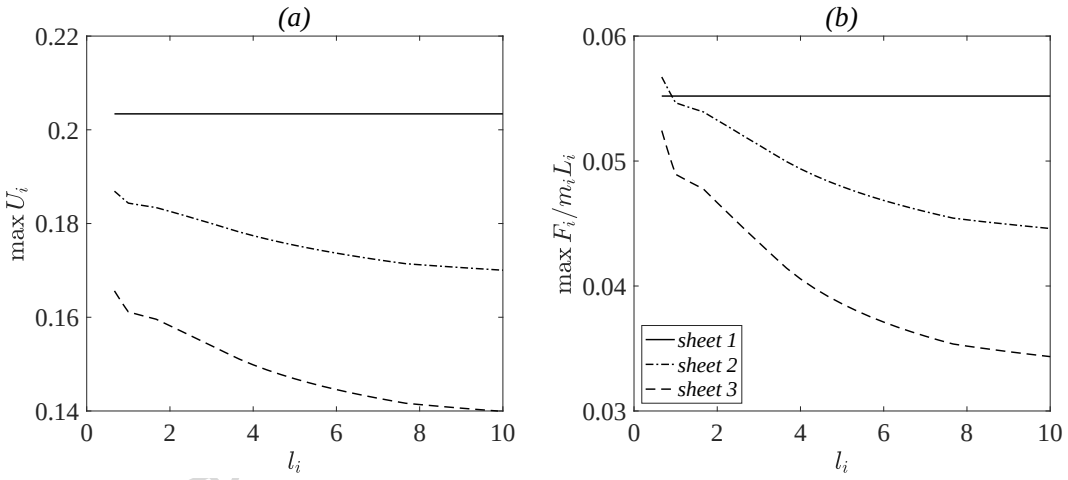

FIG. 9. Maximum values of (a) horizontal velocities and (b) horizontal forces for the set of three sheets ($L_i = 3$, $m_i = 0.1$, $D_i = 1$, $i = 1, 2, 3$) under the action of a solitary wave of amplitude $A = 0.2$ without current.

loads on sheet 1 and sheet 2 have almost equal maximums. This can be attributed to the intensified fluid motion in the open-water space between the sheets which are situated at a critical distance close to collision. The maximum horizontal velocities and forces on sheet 2 and sheet 3 decrease with an increase in the spacing parameter l_i before settling to an approximately constant value. Since the wave-induced force depends directly on the amplitude of the wave, one can say that the wave attenuates as it propagates through multiple floating sheets.

Figure 10 shows the peak values of horizontal velocity and horizontal forces against sheet sequence number in the cluster of ten sheets set at equal distances l_i to each other acted upon by a solitary wave. It is observed that, each subsequent sheet in the set experiences smaller wave-induced load and drifts with lower speed. In compact sheet cluster, the solitary wave passes over to the next sheet without casting the interaction between them and the sheet cluster drifts as a whole. In sparse sheet cluster, the wave has enough space to deform and propagate in the open water region between the sheets and to be partly reflected on encounter with each subsequent sheet. Therefore, the wave attenuates faster in the cluster with larger spacing area, but at some point, further increase of the spacing parameter has little effect on the wave transformation.

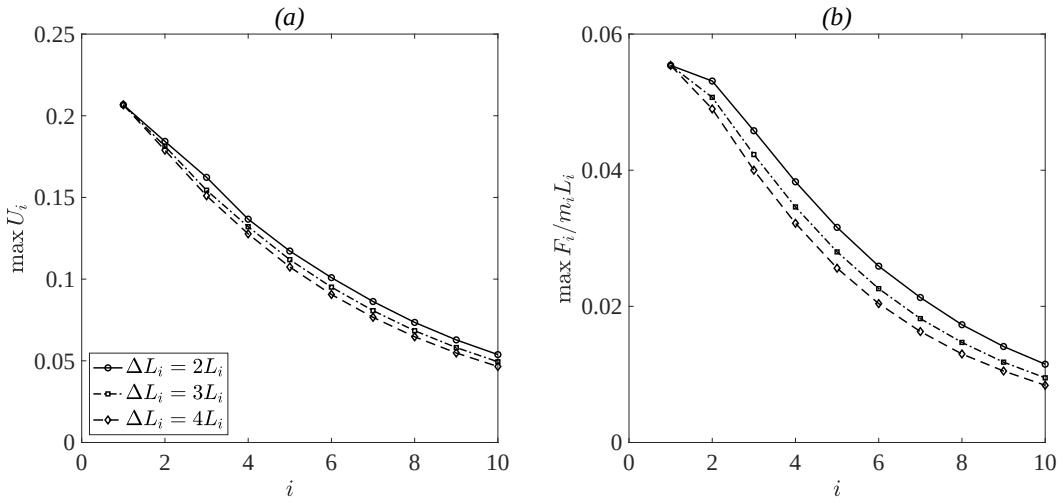

FIG. 10. Maximum values of (a) horizontal velocities and (b) horizontal forces for the set of ten sheets ($L_i = 3$, $m_i = 0.1$, $D_i = 1$, $i = 1, \ldots, 10$) with different spacing parameter l_i, $i = 1, N$ under the action of a solitary wave of amplitude $A = 0.2$ without current.

IV. VELOCITY AND PRESSURE FIELDS

A. Cnoidal wave without current

Figure 11 shows the interaction of a cnoidal wave with two free sheets, approximately when the wave crest passes the fluid space between them. Vector fields and contour plots of the fluid velocity (u, v) as well as the pressure distribution $p(x, y)$ at three successive time moments are displayed. The maximum fluid velocity is observed in the region between the sheets and under the adjacent edges. Intense fluid motions with wave resonance excited by complex hydrodynamic interactions in the gap between two floating bodies is widely observed and has been extensively investigated, see e.g. Sun et al. (2010); Lu et al. (2020). As seen in figure 11, the hydrostatic pressure is dominant in the total pressure distribution and the pressure gradient is discontinuous across the lines dividing the regions. Consequently, the fluid flows differently under different sheets, which leads to different wave forcing on the upwave and the downwave sheets.

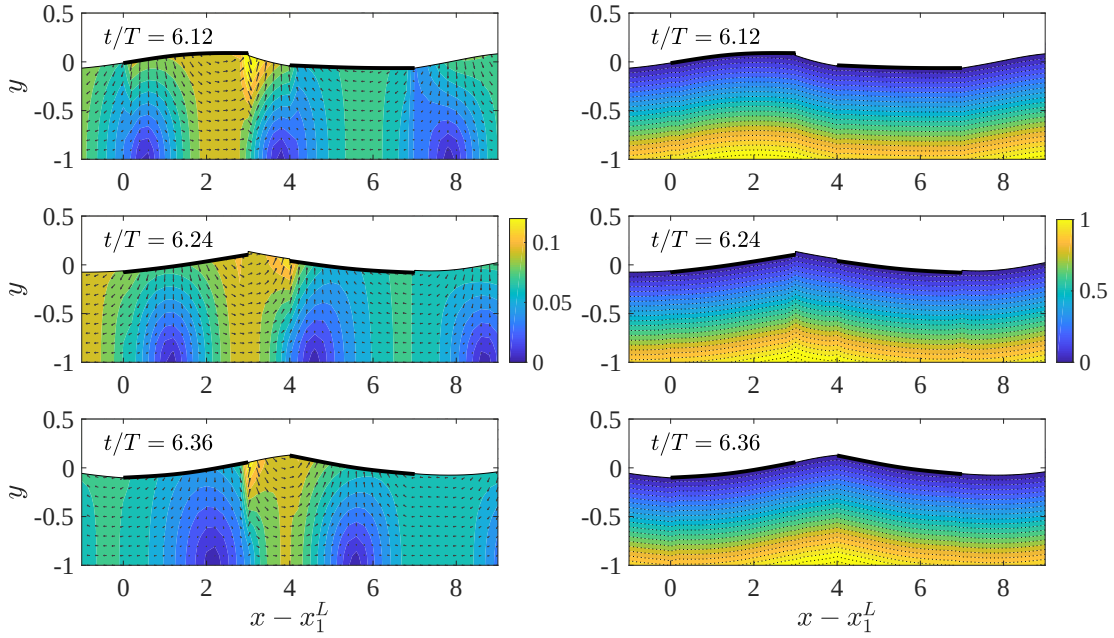

FIG. 11. Snapshots of velocity and pressure fields of cnoidal wave interaction ($H = 0.25$, $\lambda/L_1 = 2.5$, $U_c = 0$) with two free elastic sheets ($L_i = 3$, $m_i = 0.05$, $D_i = 0.1$, $i = 1, 2$) initially set at a distance $l_1 = L_1/3$ at three different time moments. Left column: vectors and dimensionless magnitude of fluid particle velocity; right column: dimensionless fluid pressure.

B. Cnoidal wave with current

Figure 12 compares the velocity fields and pressure distributions at one specific time moment for two free sheets under the action of a cnoidal wave with and without current. As shown in figure 12, both under the sheets and in the gap between them, the favourable current stimulates the flow of fluid particles towards the wave propagation, while the adverse current suppresses it. In the points where the fluid velocity is small, the current reverses the direction of fluid particles. The wave combined with positive and negative current propagates faster and slower, respectively. Further increase of the negative current is expected to lead to wave blocking.

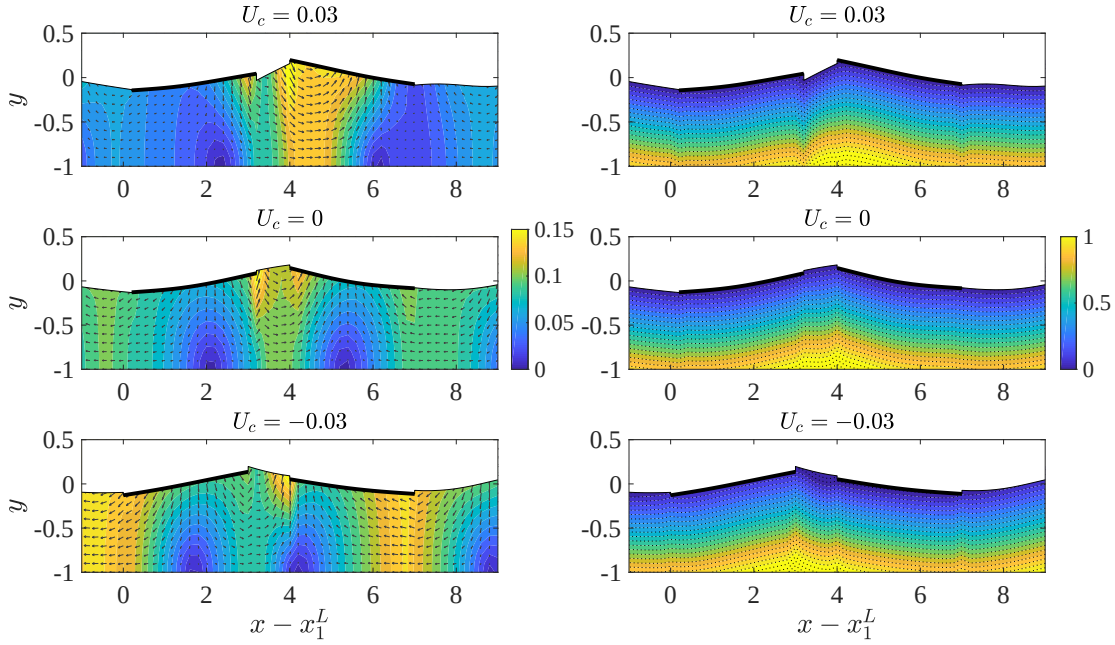

FIG. 12. Snapshots of velocity and pressure fields of interaction of a cnoidal wave ($H = 0.25$, $\lambda/L_1 = 2.5$) with and without current with two free elastic sheets ($L_i = 3$, $m_i = 0.05$, $D_i = 0.1$, $i = 1, 2$) initially set at a distance $l_1 = L_1/3$ at time $t/T = 7.32$. Left column: vectors and dimensionless magnitude of fluid particle velocity; right column: dimensionless fluid pressure.

C. Solitary wave

Figure 13 shows that the presence of fluid gap introduces insignificant disturbance into the velocity field and pressure distribution as solitary wave propagates along two floating elastic sheets, except that the trajectories of fluid particles change slightly at the trailing edges. The smallest distance between the sheets occurs when the wave crest is above the fluid gap dividing them. As the wave leaves the upstream sheet and comes into contact with the downstream sheet, the distance between them increases. In the end, the general position of the pair of sheets shifts in the direction of wave propagation and the small difference in the drifted distance is due to the gradual wave attenuation, as the wave progress along the collection of floating sheets (see figures 9-10).

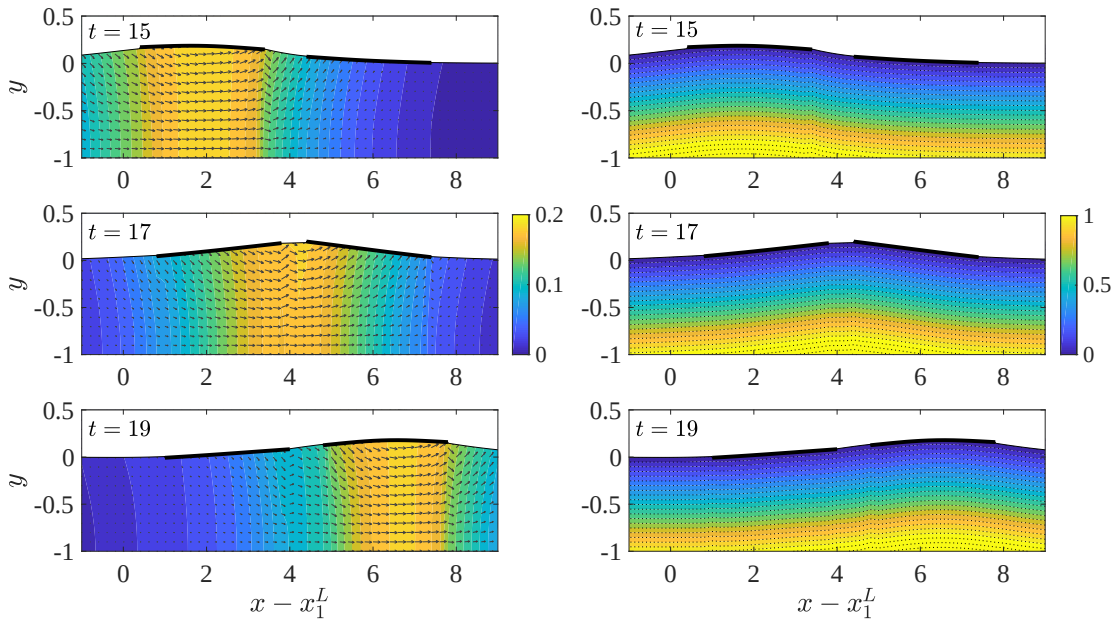

FIG. 13. Snapshots of velocity and pressure fields of solitary wave interaction ($A = 0.2$) with two free elastic sheets ($L_i = 3$, $m_i = 0.05$, $D_i = 0.1$, $i = 1, 2$) initially set at a distance $l_1 = L_1/2$ at three different time moments. Left column: vectors and dimensionless magnitude of fluid particle velocity; right column: dimensionless fluid pressure.

V. NET DRIFT SPEEDS AND SURGE OSCILLATION HEIGHTS

In Part I (Kostikov et al., 2021b), we analysed the drift response of the single sheet to regular waves in a broad range of wave parameters with the use of net drift speed and surge oscillation height. The net drift speed, U^d, was defined as the slope of a best fitting trend line of the sheet trajectory X, and the surge oscillation height, H^s, was defined as oscillation height of the periodic signal separated from the sheet trajectory. When multiple sheets are involved, it is more difficult to rely on the results obtained with the time-averaging technique. The sheets can change their drift speeds or even the drift directions, because the fluid gaps dividing them are time-dependent. Therefore, in this section, we will focus on the case of two sheets located at a relatively large distance to avoid collision and minimize changes in the drifting trends. We will consider the time intervals in which both sheets move with constant oscillation heights and periods and their relocations introduce little changes

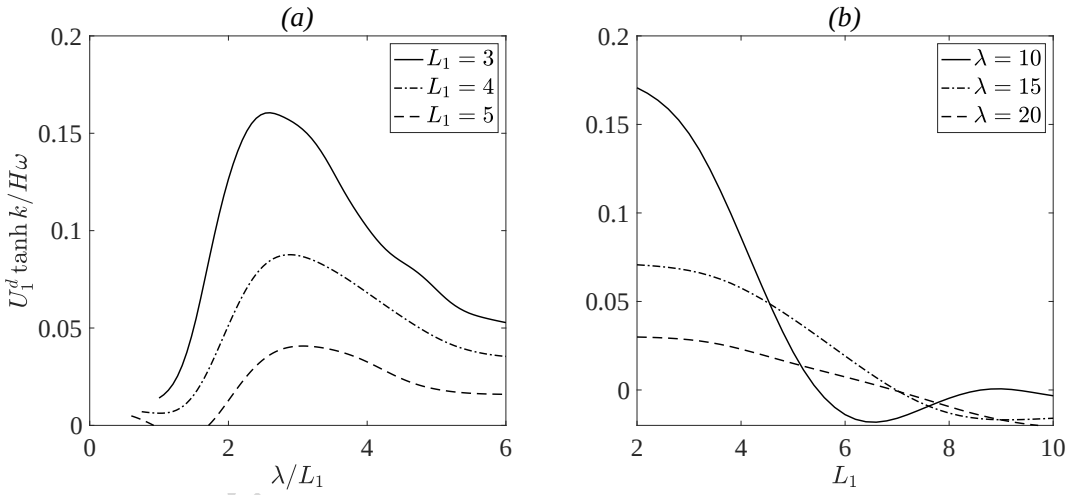

FIG. 14. Variation of net drift speed of the single sheet (a) with wavelength, λ, for various sheet lengths, and (b) with sheet length, L_1, for various wavelengths, under the action of cnoidal waves without current, ($H = 0.1$, $m_1 = 0.1$, $D_1 = 1$).

to the time-averaged quantities. Following the notation introduced earlier in Part I, the net drift speed, U_i^d, and surge oscillation height, H_i^s, of i-th sheet will be normalized with the dimensionless mean drift speed of fluid particles on the fluid surface $H\omega/\tanh k$ and their oscillation height $H/\tanh k$, respectively. Here ω and k are the frequency and wave number of the incident wave.

Figure 14 shows the net drift speed of the single sheet of various lengths under the action of various wave conditions. It is observed that the drift speed decreases rapidly and nonlinearly for longer sheets. The drift speeds of the sheets of length $L_1 > 5$ are less than 5% of the drift speed of the fluid particles on the water surface regardless of the incoming wavelength. This demonstrates the choice of the sheets length $L_i = 3$ for this study, best suitable for the analysis of the drift motion of equally-sized multiple sheets.

A. Cnoidal wave without current

In figures 15 and 16, the normalized net drift speeds and surge oscillation heights of two sheets initially located at different distances l_1 from each other are presented as continuous functions of wavelength to the sheet length ratio λ/L_1 and compared with the case of a single

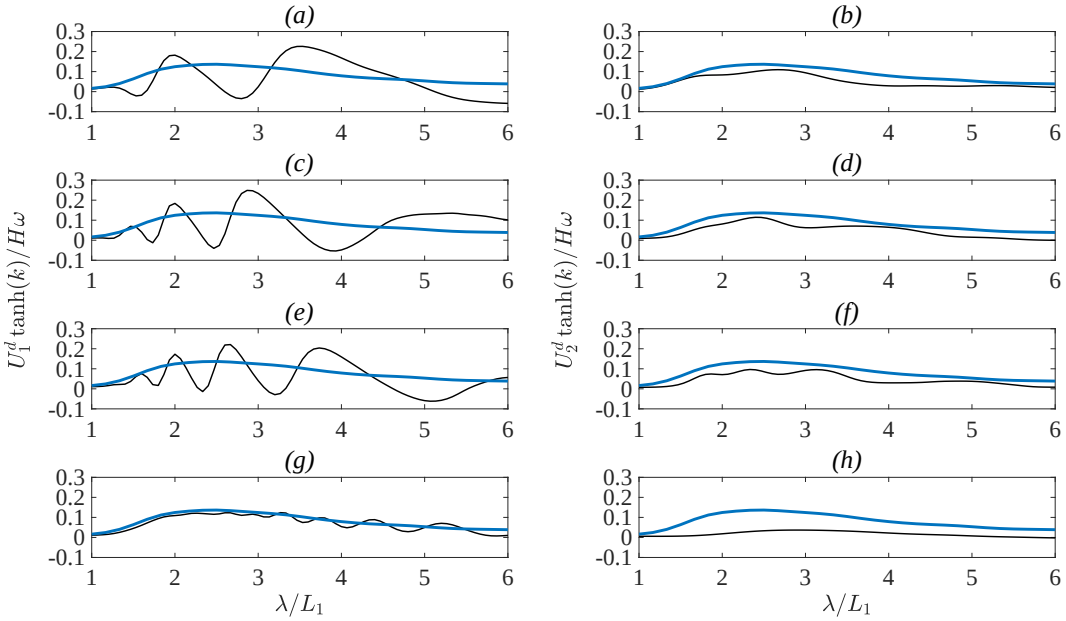

FIG. 15. Net drift speeds of sheet 1 (left column) and sheet 2 (right column) in the set of two free sheets ($L_i = 3$, $m_i = 0.1$, $D_i = 1$, $i = 1, 2$) located at initial distance: (a,b) $l_1 = L_1$, (c,d) $l_1 = 2L_1$, (e,f) $l_1 = 3L_1$, (g,h) $l_1 = 12L_1$ under the action of cnoidal waves ($H = 0.1$) without current. Thick lines corresponds to a single sheet of identical properties.

sheet. It is demonstrated that two sheets act on each other in two completely different ways. The net drift speed of the upstream sheet has multiple extrema, becoming more frequent as the distance parameter increases. When initial distance between the sheets is comparable to their lengths, the variation of the net drift speed of the upstream sheet ranges from small negative values to the values twice as large as the net drift speed of the single sheet. Compared to the single sheet, the downwave sheet exhibits the similar trend with respect to the incident wavelength, but with lower speed. As the distance between the sheets tends to infinity and the interaction between them becomes weaker, the plot of the net drift speed of the upstream sheet attains the curve, specific to the drift speed of the single sheet and the net drift speed of the downwave sheet becomes smaller. From long wave perspective, both free sheets drift with equal speeds, as it is known that longer waves are perfectly transmitted by the elastic sheets.

Yiew et al. (Yiew et al., 2017), in the laboratory experiments with two plastic disks whose

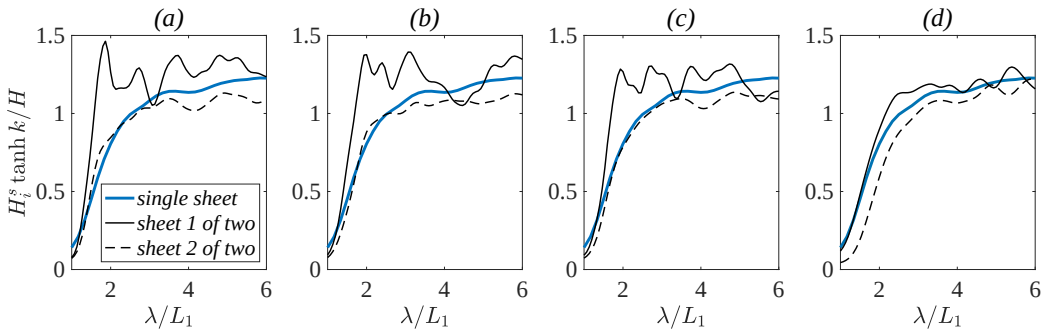

FIG. 16. Surge oscillation heights of sheet 1 and sheet 2 in the set of two free sheets ($L_i = 3$, $m_i = 0.1$, $D_i = 1$, $i = 1, 2$) located at initial distance: (a) $l_1 = L_1$, (b) $l_1 = 2L_1$, (c) $l_1 = 3L_1$, (d) $l_1 = 12L_1$ and a single sheet of identical properties under the action of cnoidal waves ($H = 0.1$) without current.

translational motion were restricted by mooring, concluded that two floating disks have no effect on each other's surge motions. Similarly, in the present study, the surge motion of the downwave sheet is consistent with the surge motion of the single sheet, differing slightly in the long wave limit, see figure 16. Just the opposite, the upstream sheet exhibits the resonant surge behaviour with increased oscillation amplitude in the short wave regime ($\lambda/L < 2.5$). This effect is due to the large drift motion induced by short waves. In fact, the phases of the waves incident on the upstream sheet and reflected from the downwave sheet can occur matched due to the rapidly changing distance between them. This way, the differential drift is originated by wave energy exchange between two sheets, which becomes more intense when the sheets are located at a close distance to each other.

B. Cnoidal wave with current

Figure 17 illustrates the effect of ambient current on drift response of two sheets located at a distance l_1 from each other by plotting the contours of their net drift speeds against two-parametric set of variables $(l_1/L_1, U_c)$. Similar to the case of a single sheet, the net drift speeds of both sheets grow with an increase in the current speed, but the rate of change depends on the incident wavelength and the distance between them. As observed in figure 17, the net drift speeds exhibit regular patterns with respect to the distance parameter

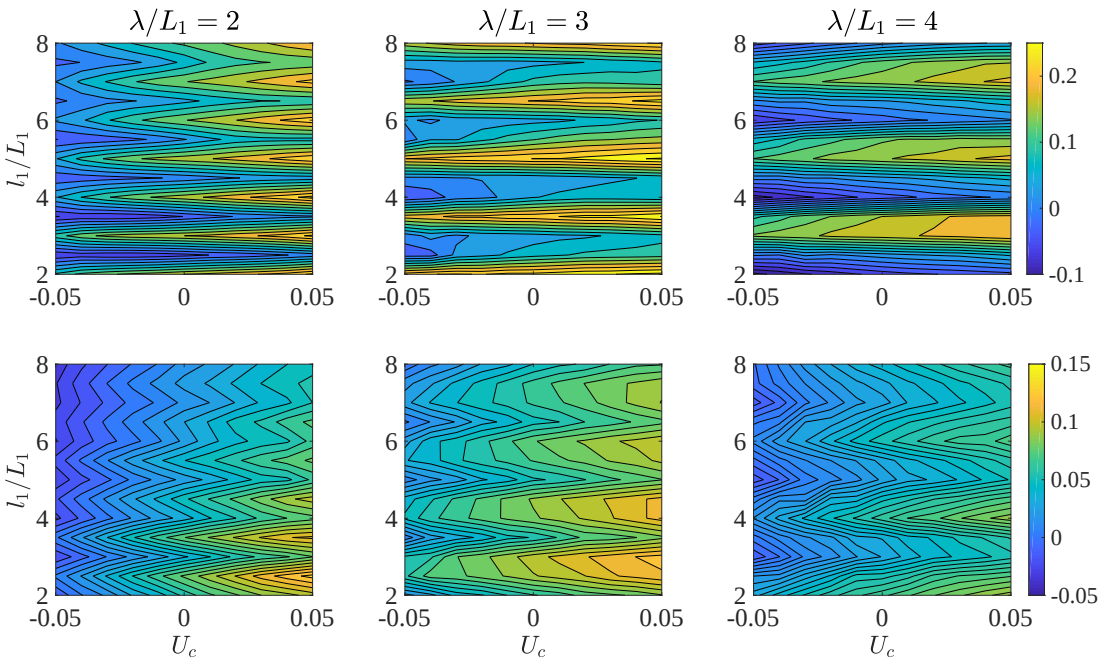

FIG. 17. Contours of the net drift speeds of two freely floating sheets ($L_i = 3$, $m_i = 0.1$, $D_i = 1$, $i = 1, 2$) under action of cnoidal waves ($H = 0.1$) of different wavelength λ with and without current: (upper row) $U_1^d \tanh(k)/H\omega$; (lower row) $U_2^d \tanh(k)/H\omega$.

l_1, which periods grow with wavelength λ. Increasing distance has decreasing effect on correlation between the speed of the current and the speeds of the sheets drift.

VI. WAVE REFLECTION AND TRANSMISSION

To date, the analysis on reflection and transmission coefficients has been held for collections of floating plates (Kostikov et al., 2021a) or a plate with a finite series of cracks (Porter and Evans, 2006; Kohout et al., 2007), restrained from moving horizontally. This section is concerned with the scattering of an incident wave by different configurations of multiple sheets and analyze the effect of free drift on reflection and transmission coefficients. The coefficients c_R and c_T give the proportion of the wave energy reflected and transmitted by the group of sheets as:

$$c_R = \frac{a_R}{a_I}, \quad c_T = \frac{a_T}{a_I}, \tag{23}$$

where amplitudes of the incident a_I, reflected a_R and transmitted a_T waves are separated by the method of Grue (Grue, 1992) from the signals at two gauges upwave and two gauges downwave. We use the Fourier transform to extract the fundamental harmonics from nonlinear wave profiles, which is sufficient for estimation of reflection and transmission coefficients. This method has been applied successfully in Level I GN models for submerged horizontal plate (Hayatdavoodi et al., 2017) and multiple deformable sheets (Kostikov et al., 2021a). For the detailed description of the coefficients the reader is referenced to these papers.

A. Cnoidal wave without current

Figure 18 shows the variation of reflection c_R and transmission c_T coefficients versus incident wavelength to sheet length ratio λ/L_1 for two sheets in two modes: horizontally fixed and drifting freely. Four cases, differing by spacing parameter l_1, are displayed. It is demonstrated that reflection coefficient of two sheets depends strongly on the distance between them. As expected, figure 18 depicts the decrease in reflection and increase in transmission coefficients as wavelength is increased. In the long wave limit, the plate system reaches maximum wave transmission. Features in the plots are due to the presence of fluid gap between the sheets. With increase in the spacing area the points of minimum reflection have the tendency to multiply and, because of the diminishing influence of the downwave sheet, the plot of reflection coefficient attains the form featured by a single sheet. The transmission coefficient is less sensitive to the change in the distance parameter and grows slower in the short wave region with the distancing of the downwave sheet.

In Part I two distinct wave regimes were discovered: short wave regime where the free sheet drifts with high speed exhibiting little surge motion; and long wave regime where the surge motion of the sheet is dominant and the drift speed is relatively small. The same two regimes are observed for multiple sheets in terms of wave reflection. Compared to their fixed counterparts, two free sheets produce weaker reflection for short waves ($\lambda/L_1 < 2.5$), but stronger reflection for long waves ($\lambda/L_1 > 2.5$), see figure 18. The drift effect is of increasing importance as wavelength is increased, except for the short wave region and points of minimum wave reflection. Thus, it can be concluded that surge motion of the sheets facilitates wave reflection, while their translatory motion acts just the opposite. Nelli

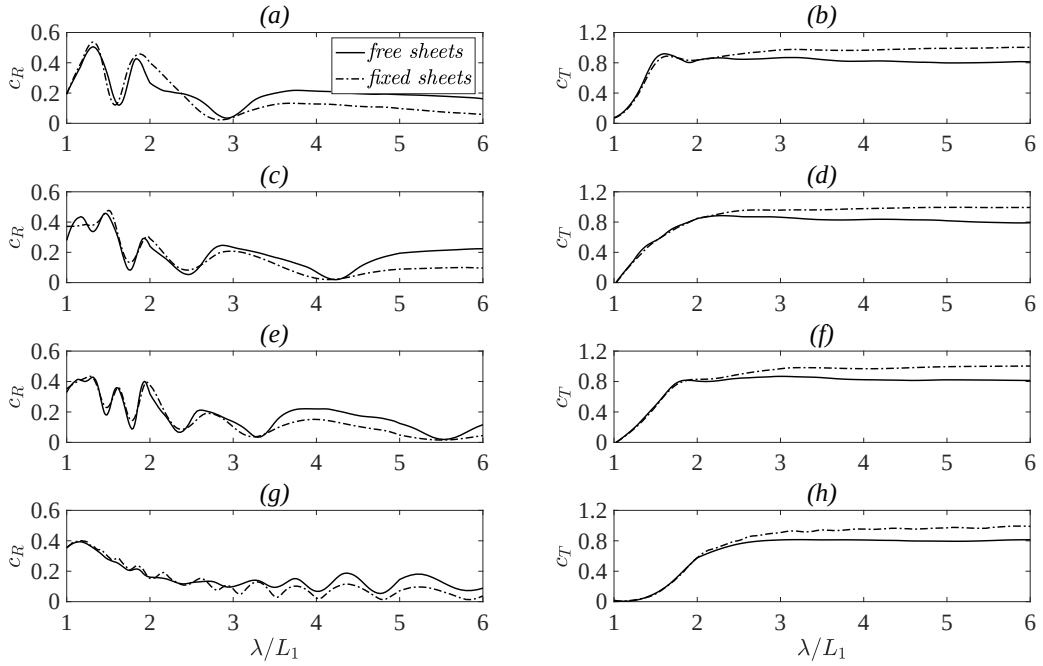

FIG. 18. Reflection c_R (left column) and transmission c_T (right column) coefficients for free and fixed set of two sheets ($L_i = 3$, $m_i = 0.1$, $D_i = 1$, $i = 1, 2$) located at an initial distance (a,b) $l_1 = L_1$; (c,d) $l_1 = 2L_1$; (e,f) $l_1 = 3L_1$; (g,h) $l_1 = 12L_1$.

et al. (2017) established experimentally the same result that wave reflection of the freely floating plate is smaller than that of the moored plate with or without edge barriers. In their experiments, the wavelength to plate length ratios ($\lambda/L = 1, 1.26, 1.56$) correspond to the short wave regime of the present study.

Figure 19 presents the contours of reflection coefficient c_R for the set of three sheets in a wide range of spacings parameters l_1 and l_2 for different incoming waves. For the short wave ($\lambda/L_1 = 2$), the reflection coefficient maxima are arranged in a periodical pattern in the neighbourhood of the points $(l_1/L_1, l_2/L_1) = \{(1,1), (1,3), (3,1), (3,3), ...\}$. The distances between adjacent peaks of the contours in figure 19 increase with an increase in wavelength ($\lambda/L_1 = 3, 4$). This is an interesting observation, as it is known that a single sheet experiences minimum wave reflection when the incoming wavelength matches the length of the plate.

In figure 20, the reflection coefficient c_R for the set of ten equally-spaced sheets is plotted

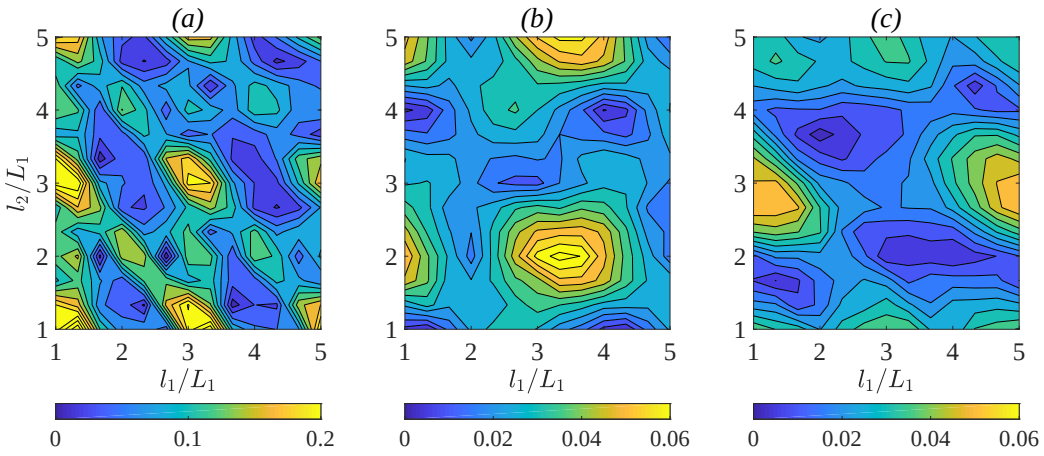

FIG. 19. Contour plots for the variation of reflection coefficient c_R as a function of distance parameters l_1 and l_2 for three free sheets ($L_i = 3$, $m_i = 0.1$, $D_i = 1$, $i = 1, 2, 3$) under the action of a cnoidal wave: (a) $\lambda/L_1 = 2$; (b) $\lambda/L_1 = 3$; (c) $\lambda/L_1 = 4$.

against wavelength to sheet length ratio λ/L_1. Two sets of fixed and free sheets with two different initial spacing parameters l_i are considered. Because of the initially recurring structure of the floating sheet cluster, for wavelengths λ divisible by L_i+l_i, the sheets respond to the incoming wave in a similar way and the reflection coefficients reaches local maximums. The extremum points in the shorter wave spectrum ($\lambda/L_1 < 2.5$) can be attributed to the smaller scale symmetric features of the sheet cluster: the same pattern, but inversely oriented, repeats at an interval $L_i + l_i/2$. Thus, figure 20 demonstrates that the spacing parameter l_i plays an important role in the process of wave scattering. The effect of free drift, observed for two sheets in figure 18, holds true for multiple sets of sheets and exhibits a similar growing trend with increasing wavelength.

Figure 21 shows how the reflection coefficient c_R for the initially uniform sheet cluster changes with the number of elements N. Three incoming waves are displayed, which correspond to the wave regimes with the highest wave reflection in case of ten sheets ($N = 10$), shown in figure 20(a). It is observed in figure 21 that in small sheet clusters (when $N < 5$), the wave reflection increases rapidly with addition of sheets to the cluster. In the larger clusters ($N \geq 5$), however, the addition of new elements introduces little to no changes to the wave reflection. The effect of free drift is stronger in multiple sets of sheets under

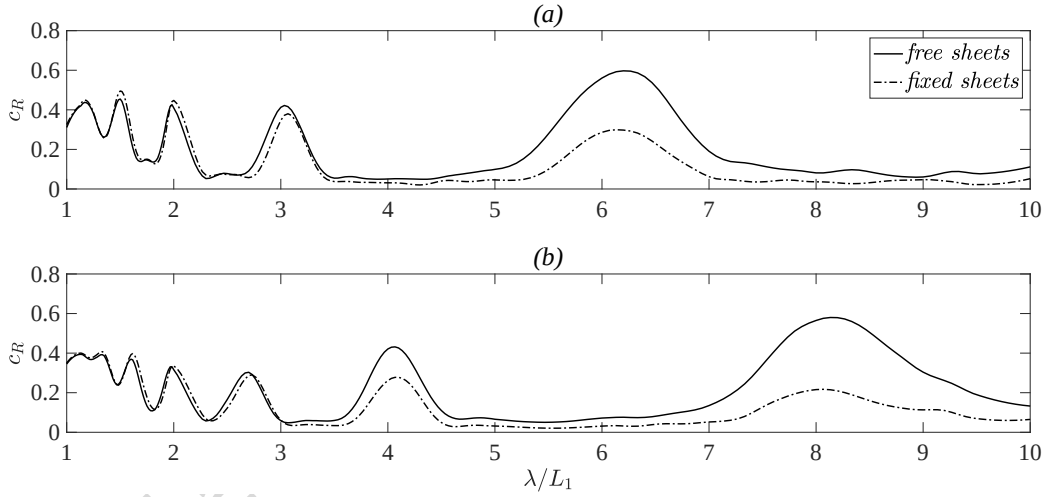

FIG. 20. Reflection coefficient c_R for free and fixed set of ten sheets ($L_i = 3$, $m_i = 0.1$, $D_i = 1$, $i = 1, \ldots, 10$) located at an initial distance (a) $l_i = 2L_1$, (b) $l_i = 3L_1$, $i = 1, \ldots, 9$.

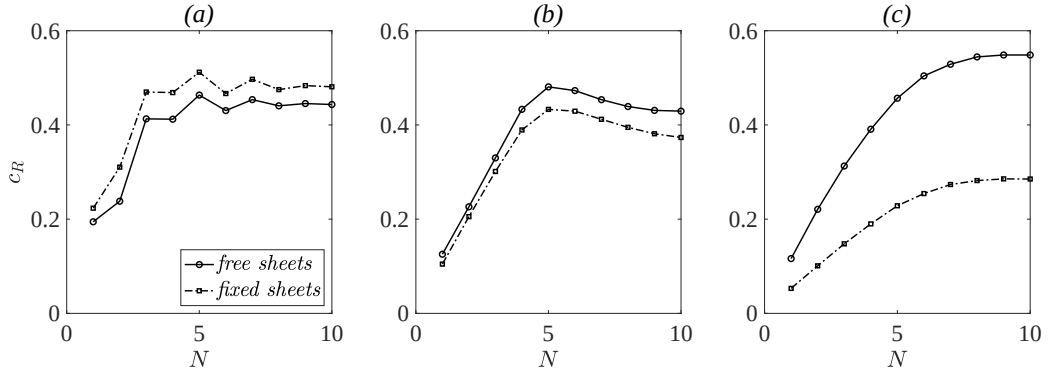

FIG. 21. Reflection coefficient c_R for the sets of free and fixed sheets ($L_i = 3$, $m_i = 0.1$, $D_i = 1$, $i = 1, \ldots, N$) initially located at a distance $l_i = 2L_1$ for various number of sheets N under action of a cnoidal wave of length (a) $\lambda/L_1 = 2$, (b) $\lambda/L_1 = 3$, (c) $\lambda/L_1 = 6$ for different number N.

the action of longer waves. Figure 21 confirms that in any collection of sheets, regardless of their number N and relative position, the free drift reduces the wave reflection slightly for short waves ($\lambda/L_1 < 2.5$), and increases the wave reflection considerably for long waves ($\lambda/L_1 > 2.5$).

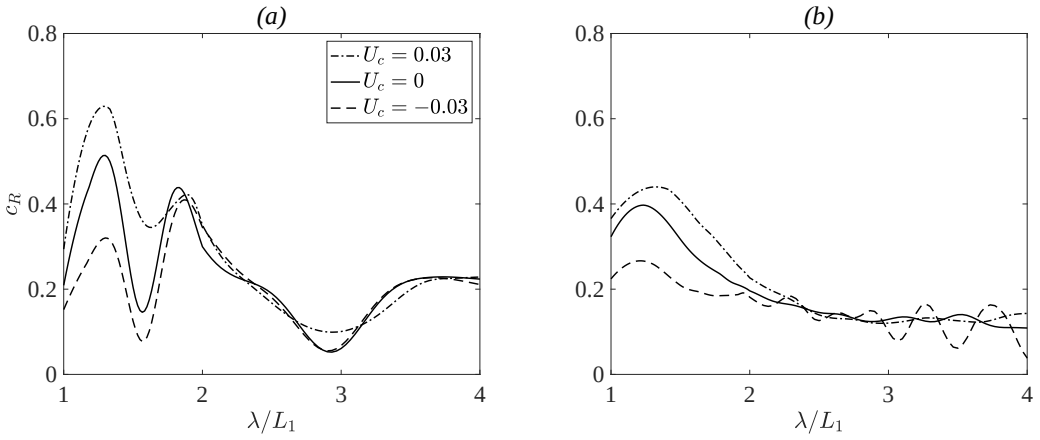

FIG. 22. Reflection coefficient c_R for free set of two sheets ($L_i = 3$, $m_i = 0.1$, $D_i = 1$, $i = 1, 2$) initially located at a distance (a) $l_1 = L_1$; (b) $l_1 = 12L_1$ under the action of cnoidal waves with and without current.

B. Cnoidal wave with current

Figure 22 illustrates the effect of current on reflection coefficient of two freely floating sheets located close to each other ($l_1 = L_1$) or at a large distance ($l_1 = 12L_1$) in a range of wavelength to sheet length ratios λ/L_1. As seen in figure 22, the favourable current facilitates wave reflection, while the adverse current works just the opposite. The presence of current has sufficient effect on wave reflection for short waves only ($\lambda/L < 2.5$). For longer waves ($\lambda/L_1 > 2.5$), the reflection coefficient is invariant with the presence of current, regardless of its direction and speed, as well as the distance between the sheets.

VII. CONCLUSIONS

In this paper, a nonlinear two-dimensional model of interaction of waves and current with a finite set of fixed and freely floating deformable sheets without overwash is presented. The model performance has been investigated in view of the drift motion of the sheets in the range of incident wave parameters, current speeds, number of sheets and distances between them. The sheets in a set exhibit different drift behaviour because of the phase difference in the wave fields driving them. We have discovered that differential drift of the sheets is determined by the interplay between wavelength, sheets length and initial spacing parameter.

Extensive results are provided for the effects of free drift on the sheet response to the wave and current actions, from which the following conclusions can be drawn: (i) multiple sheets can be grouped into bands by the repeated wave passage (herding effect); (ii) the upwave sheet acts on the downwave sheet by decreasing its drift speed; (iii) the downwave sheet acts on the upwave sheet by modulating its drift speed, depending on wavelength and distance between them; (iv) two sheets surge motions are independent, except for short waves under which the upwave sheet may oscillate with increased amplitude; (v) the ability of the sheets to drift reduces wave reflection under action of short waves ($\lambda/L_1 < 2.5$), and increases wave reflection under the action of long waves ($\lambda/L_1 > 2.5$); (vi) the effect of free drift on the reflection coefficient is of increasing magnitude for larger number of sheets and longer wavelength; (vii) the stimulating and suppressing effects of the current on the drift motion is non-uniformly distributed between the floating sheets.

The above-formulated conclusions were obtained for uniformly spaced arrays of equally-sized sheets of equal properties, floating freely on the water surface. It may be expected, that similar list of conclusions without loss of generality may be applied to the sets of arbitrary-sized and arbitrary-spaced sheets, although this needs to be shown.

Data Availability Statement: The data that supports the findings of this study are available within the article.

REFERENCES

Amdahl, J. (2019). Impact from ice floes and iceberges on ships and offshore structures in polar regions. *IOP Conf. Ser.: Mater. Sci. Eng.*, 700:012039.

Barman, S. C., Das, S., Sahoo, T., and Meylan, M. H. (2021). Scattering of flexural-gravity waves by a crack in a floating ice sheet due to mode conversion during blocking. *J. Fluid Mech.*, 916(A11):1–28.

Bennetts, L. G. and Williams, T. D. (2015). Water wave transmission by an array of floating discs. *Proc. R. Soc. A*, 471:20140698.

Das, S., Kar, P., Sahoo, T., and Meylan, M. (2018a). Flexural-gravity wave motion in the presence of shear current: wave blocking and negative energy waves. *Phys. Fluids*, 30:106606.

Das, S., Sahoo, T., and Meylan, M. H. (2018b). Dynamics of flexural gravity waves: from sea ice to hawking radiation and analogue gravity. *Proc. R. Soc. A.*, 474:20170223.

Ertekin, R. C. (1984). Soliton generation by moving disturbances in shallow water: theory, computation and experiment. *PhD thesis, University of California at Berkeley.*, page 352.

Ertekin, R. C. and Becker, J. M. (1998). Nonlinear diffraction of waves by a submerged shelf in shallow water. *J. Offshore Mech. Arct.*, 120:212–220.

Ertekin, R. C., Hayatdavoodi, M., and Kim, J. W. (2014). On some solitary and cnoidal wave diffraction solutions of the Green-Naghdi equations. *Applied Ocean Research*, 47:pp. 125–137.

Ertekin, R. C., Webster, W. C., and Wehausen, J. W. (1986). Waves caused by a moving disturbance in a shallow channel of finite width. *J. Fluid Mech.*, 169:275–292.

Ertekin, R. C. and Xia, D. (2014). Hydroelastic response of a floating runway to cnoidal waves. *Phys. Fluids*, 26:027101.

Feltham, D. (2015). Arctic sea ice reduction: the evidence, models and impacts. *Phil. Trans. R. Soc. A.*, 373:20140171.

Green, A. E., Laws, N., and Naghdi, P. M. (1974). On the theory of water waves. *Proc. R. Soc. Lond. A.*, 338:43–55.

Green, A. E. and Naghdi, P. M. (1976a). A derivation of equations for wave propagation in water of variable depth. *J. Fluid Mech.*, 78:237–246.

Green, A. E. and Naghdi, P. M. (1976b). Directed fluid sheets. *Proc. R. Soc. Lond. A.*, 347:447–473.

Grotmaack, R. and Meylan, M. H. (2006). Wave forcing of small floating bodies. *J. Waterw., Port, Coastal, Ocean Eng.*, 132(3):192–198.

Grue, J. (1992). Nonlinear water waves at a submerged obstacle or bottom topography. *J. Fluid Mech.*, 244:455–476.

Harms, V. W. (1987). Steady wave-drift of modeled ice floes. *J. Waterw. Port Coast Ocean Eng., ASCE*, 113(6):606–622.

Hayatdavoodi, M. and Ertekin, R. C. (2015a). Nonlinear wave loads on a submerged deck by the Green-Naghdi equations. *J. Offshore Mech. Arct.*, 137(1):11102.

Hayatdavoodi, M. and Ertekin, R. C. (2015b). Wave forces on a submerged horizontal plate – part I: Theory and modelling. *J. Fluids Struct.*, 54:566–579.

Hayatdavoodi, M. and Ertekin, R. C. (2015c). Wave forces on a submerged horizontal plate – part II: Solitary and cnoidal waves. *J. Fluids Struct.*, 54:580–596.

Hayatdavoodi, M., Ertekin, R. C., Robertson, I. N., and Riggs, H. R. (2015). Vulnerability assessment of coastal bridges on oahu impacted by storm surge and waves. *Natural Hazards*, 79(2):1133–1157.

Hayatdavoodi, M., Ertekin, R. C., and Valentine, B. D. (2017). Solitary and cnoidal wave scattering by a submerged horizontal plate in shallow water. *AIP Adv*, 7:065212–29.

Hayatdavoodi, M., Neil, D. R., and Ertekin, R. C. (2018). Diffraction of cnoidal waves by vertical cylinders in shallow water. *Theor. Comp. Fluid. Dyn.*, 32(5):561–591.

Hayatdavoodi, M., Treichel, K., and Ertekin, R. C. (2019). Parametric study of nonlinear wave loads on submerged decks in shallow water. *J. Fluids Struct.*, 86:266–289.

Herman, A. (2011). Molecular-dynamics simulation of clustering processes in sea-ice floes. *Phys. Rev. E*, 84:056104.

Herman, A. (2018). Wave-induced surge motion and collisions of sea ice floes: finite-floe-size effects. *J. Geophys. Res.: Oceans*, 123:7472–7494.

Kar, P., Sahoo, T., and Meylan, M. (2020). Bragg scattering of long waves by an array of floating flexible plates in the presence of multiple submerged trenches. *Phys. Fluids*, 32:096603.

Kim, J. W., Bai, K. J., Ertekin, R. C., and Webster, W. C. (2001). A derivation of the

Green-Naghdi equations for irrotational flows. *J. Engineering Mathematics*, 40:pp. 17–42.

Kim, J. W. and Ertekin, R. C. (2000). A numerical study of nonlinear wave interaction in irregular seas: Irrotational Green-Naghdi model. *Marine Structures*, 13:pp. 331–348.

Kohout, A. L., Meylan, M. H., Sakai, S., Hanai, K., Leman, P., and Brossard, D. (2007). Linear water wave propagation through multiple floating elastic plates of variable properties. *J. Fluids Struct.*, 23:649–663.

Kostikov, V., Hayatdavoodi, M., and Ertekin, R. C. (2021a). Hydroelastic interaction of nonlinear waves with floating sheets. *Theor. Comput. Fluid Dyn.*, 35:515–537.

Kostikov, V. K., Hayatdavoodi, M., and Ertekin, R. C. (2021b). Drift of elastic floating ice sheets by waves and current, part i: single sheet. *Proc. Roy. Soc. A.*, 477:20210449.

López, M., Rodriguez, N., and Iglesias, G. (2021). Combined floating offshore wind and solar pv. *J. Mar. Sci. Eng.*, 8(576):1–20.

Lu, L., Tan, L., Zhou, Z., and Zhao, M. (2020). Two-dimensional numerical study of gap resonance coupling with motions of floating body moored close to a bottom-mounted wall. *Phys. Fluids*, 32:092101.

McGovern, D. J. and Bai, W. (2014). Experimental study on kinematics of sea ice floes in regular waves. *Cold Reg. Sci. Technol.*, 103:15–30.

Meylan, M. H., Yeiw, L. J., Bennetts, L. G., French, B. J., and Thomas, G. A. (2015). Surge motion of an ice floe in waves: comparison of a theoretical and an experimental model. *Ann. Glaciol.*, 56(69):155–159.

Montiel, F., Bonnefoy, F., Ferrant, P., Bennetts, L. G., Squire, V. A., and Marsault, P. (2013). Hydroelastic response of floating elastic disks to regular waves. part 1. wave basing experiments. *J. Fluid Mech.*, 723:604–628.

Neill, D. R., Hayatdavoodi, M., and Ertekin, R. C. (2018). On solitary wave diffraction by multiple, in-line vertical cylinders. *Nonlinear Dynamics*, 91(2):975–994.

Nelli, F., Bennetts, L., Skene, D., Monty, J., Lee, J., Meylan, M., and Toffoli, A. (2017). Reflection and transmission of regular water waves by a thin, floating plate. *Wave Motion*, 70:209–221.

Ogasawara, T. and Sakai, S. (2006). Numerical analysis of the characteristics of waves propagating in arbitrary ice-covered sea. *Ann. Glaciol.*, 44:95100.

Porter, R. and Evans, D. V. (2006). Scattering of flexural waves by multiple narrow cracks

in ice sheets floating on water. *Wave Motion*, 43:425–443.

Ren, B., Ming, H., Dong, P., and Wen, H. (2015). Nonlinear simulations of wave-induced motions of a freely floating body using WCSPH method. *Appl. Ocean Res.*, 50:1–12.

Rottier, P. J. (1992). Floe pair interaction event rates in the marginal ice zones. *J. Geophys. Res.*, 97:9391–9400.

Shen, H. H. and Ackley, S. F. (1991). A one-dimensional model for wave-induced ice-floe collisions. *Ann. Glaciol.*, 15:87–95.

Sun, L., Taylor, R., and Taylor, P. (2010). First- and second-order analysis of resonant waves between adjacent barges. *J. Fluids Struct.*, 26:954–978.

Sun, X. (1991). Some theoretical and numerical studies on two-dimensional cnoidal-wave-diffraction problems. Master's thesis, Department of Ocean Engineering, University of Hawaii at Manoa, Honolulu, xii+149 pp.

Tavakoli, S. and Babanin, A. (2021). Wave energy attenuation by drifting and non-drifting floating rigid plates. *Ocean Eng.*, 226:108717.

Timoshenko, S. P. and Woinowsky-Krieger, S. (1959). *Theory of plates and shells*. McGraw-Hill, NY.

Wadhams, P. (1983). A mechanism for the formation of ice edge bands. *J. Geophys. Res.*, 88(C5):2813–2818.

Wang, C., Song, M., Guo, C., Wang, S., Tian, T., and Luo, W. (2020a). Experimental study of sea ice motion in waves. *Cold Reg. Sci. Technol.*

Wang, Z., Zhao, B.-b., Duan, W.-y., Ertekin, R. C., Hayatdavoodi, M., and Zhang, T.-y. (2020b). On solitary wave in nonuniform shear currents. *Journal of Hydrodynamics*, 32(4):800–805.

Wu, T., Luo, W., Jiang, D., Deng, R., and Huang, S. (2021). Numerical study on wave-ice interaction in the marginal ice zone. *J. Mar. Sci. Eng.*, 24(4):527–540.

Xia, D., Ertekin, R. C., and Kim, J. W. (2008). Fluid-structure interaction between a two-dimensional mat-type VLFS and solitary waves by the Green-Naghdi theory. *J. Fluids Struct.*, 24(4):527–540.

Yiew, D., Bennetts, L. G., Meylan, M. H., Thomas, G. A., and French, B. J. (2017). Wave-induced collisions of thin floating disks. *Phys. Fluids*, 29:127102.

Zhao, B., Wang, Z., Duan, W., Ertekin, R. C., Hayatdavoodi, M., and Zhang, T. (2020).

749 Experimental and numerical studies on internal solitary waves with a free surface. *Journal*
750 *of Fluid Mechanics*, 899.
751 Zhao, B. B., Duan, W. Y., Ertekin, R. C., and Hayatdavoodi, M. (2015). High-level Green–
752 Naghdi wave models for nonlinear wave transformation in three dimensions. *Journal of*
753 *Ocean Engineering and Marine Energy*, 1(2):121–132.
754 Zhao, B. B., Ertekin, R. C., Duan, W. Y., and Hayatdavoodi, M. (2014). On the steady
755 solitary-wave solution of the Green–Naghdi equations of different levels. *Wave Motion*,
756 51(8):1382–1395.
757 Zhao, B. B., Zhang, T. Y., Wang, Z., Duan, W. Y., Ertekin, R. C., and Hayatdavoodi, M.
758 (2019). Application of three-dimensional IGN-2 equations to wave diffraction problems.
759 *J. Ocean. Eng. Mar. Energy*, 5(4):351363.
760 Zheng, S., Meylan, M. H., Zhu, G., Greaves, D., and Iglesias, G. (2020). Hydroelastic
761 interaction between water waves and an array of circular floating porous elastic plates. *J.*
762 *Fluid Mech.*, 900:A20.